Acta Mechanica Sinica (2014) 30(6):889–900
DOI 10.1007/s10409-014-0119-5

RESEARCH PAPER

Influences of aerodynamic loads on hunting stability of high-speed railway vehicles and parameter studies

Xiao-Hui Zeng · Han Wu · Jiang Lai · Hong-Zhi Sheng

Received: 25 September 2014 / Revised: 19 November 2014 / Accepted: 31 December 2014

Abstract The influences of steady aerodynamic loads on hunting stability of high-speed railway vehicles were investigated in this study. A mechanism is suggested to explain the change of hunting behavior due to actions of aerodynamic loads: the aerodynamic loads can change the position of vehicle system (consequently the contact relations), the wheel/rail normal contact forces, the gravitational restoring forces/moments and the creep forces/moments. A mathematical model for hunting stability incorporating such influences was developed. A computer program capable of incorporating the effects of aerodynamic loads based on the model was written, and the critical speeds were calculated using this program. The dependences of linear and nonlinear critical speeds on suspension parameters considering aerodynamic loads were analyzed by using the orthogonal test method, the results were also compared with the situations without aerodynamic loads. It is shown that the most dominant factors affecting linear and nonlinear critical speeds are different whether the aerodynamic loads considered or not. The damping of yaw damper is the most dominant influencing factor for linear critical speeds, while the damping of lateral damper is most dominant for nonlinear ones. When the influences of aerodynamic loads are considered, the linear critical speeds decrease with the rise of cross wind velocity, whereas it is not the case for the nonlinear critical speeds. The variation trends of critical speeds with suspension parameters can be significantly changed by aerodynamic loads. Combined actions of aerodynamic loads and suspension parameters also affect the critical speeds. The effects of such joint action are more obvious for nonlinear critical speeds.

Keywords Hunting stability · Linear critical speed · Nonlinear critical speed · Aerodynamic loads · Suspension parameters · Orthogonal experimental design

1 Introduction

Hunting of railway vehicles is a typical kind of self-excited oscillation. The critical speed at which railway vehicles experience violent oscillations is a crucial criterion for safety design, because in such circumstances the oscillations may damage wheels and tracks, or even cause derailment. Hunting stability is hence an important problem for running dynamics of railway vehicles. The railway vehicle system can be described as a mechanical dissipative multi-body system which is fundamentally nonlinear. The nonlinear factors include nonlinear wheel/rail geometric constraints (wheel/rail contact nonlinearity), nonlinear creep force and nonlinear suspension system etc. Although the dynamical system of railway vehicles is actually nonlinear, a linear system (as a special case of the nonlinear one) can be obtained by using linearization and simplifying assumptions. The studies on hunting stability can consequently be roughly classified into two categories: linear stability and nonlinear stability.

Many works have been conducted in the area of linear hunting stability of railway vehicle. Kim et al. [1] and Cheng et al. [2–4] studied the linear stability characters of railway vehicle, and analyzed the influence of suspension parameters on linear critical speed. Hirotsu et al. [5] analyzed the influence of yaw damper, primary suspension stiffness and conicity of wheel tread on linear critical speed. Cheng et al. [6–8] and Liu et al. [9] evaluated the linear critical speed of railway vehicle on a curved track, then investigated the influence of

The project was supported by the National Basic Research Program (973 Program) of China (2011CB711100 and 2014CB046801), the National Natural Science Foundation of China (11072246 and 51490673), and the Knowledge Innovation Program of Chinese Academy of Sciences (KJCX2-EW-L01).

X.-H. Zeng (✉) · H. Wu · J. Lai · H.-Z. Sheng
Key Laboratory for Mechanics in Fluid Solid Coupling Systems, Institute of Mechanics, Chinese Academy of Sciences, 100190 Beijing, China
e-mail: zxh@imech.ac.cn

suspension parameters, curve radius and other factors on the linear critical speed. Wang and Liao [10] studied the advantage of a mechanical structure to lateral stability according to this method. Dukkipati and Narayana Swamy [11, 12] studied the lateral stability of unconventional rail trucks, and investigated the compatibility of stability and curve performance.

However, for a nonlinear vehicle system, hunting motion may occur below the linear critical speed [13, 14]. True [15] defined the nonlinear critical speed v_c in such a way that it is theoretically guaranteed that no hunting motion can take place at speeds below the speed v_c. He thought the nonlinear critical speed should be taken as the criterion of the limited speed.

The nonlinear hunting stability is one of the key problems in railway vehicle dynamics. There have been many studies on this subject. True et al. [16, 17] described the basic theory about bifurcation analysis of nonlinear vehicle system. He pointed out the right way for determining the nonlinear critical speed is to find the smallest bifurcation point by the path-following method. Hirotsu et al. [5] calculated the limit cycles varying with vehicle speed, and showed the difference between the case with yaw damper and the case without yaw damper. True et al. [18, 19] studied the chaos and asymmetry hunting in railway vehicle dynamics. Stichel [20] also studied the phenomenon of chaos. In addition, True and Jensen [21] presented bifurcation diagrams and investigate the dynamics of bogie model with realistic wheel and rail profiles. They found speed ranges with asymptotically stable forward motion along the track centre line, coexisting attractors, symmetric and asymmetric oscillations and chaos. Kim and Seok [22] performed a bifurcation analysis on a nonlinear railway vehicle having dual-bogies to examine the coupling effect of the bogies on the vehicle's hunting behavior. Polach and Kaiser [23] analyzed the hunting behavior of vehicle system using two different methods: path-following method and brute-force method. The results using these two methods are compared. The investigation shows that the path-following method can not handle the quasi-periodic motions, and the brute-force method allows an assessment of an unstable attractor. Di Gialleonardo, Braghin and Bruni [24] investigated the influence of different rail models (rigid model, simplified sectional model and Finite element model) on bifurcation diagram. Zeng [25] and Dong et al. [26] obtained the bifurcation diagrams of vehicle system by the shooting method. Dong et al. [26] performed a widely analysis on bifurcation characteristic of the CRH vehicles. The studies mentioned above are connected with a vehicle running along a straight track. In fact, the constraint of curved track makes the creep relationship and equilibrium position changed a lot, which makes the hunting stability on a curved track different from that on a straight track. Zboinski and Dusza [27–30] obtained the bifurcation diagrams, and conducted a lot of studies on the nonlinear stability of railway vehicle running on a curved track. Zeng and Wu [31] studied the critical speed at the hopf bifurcation point on circular curved track. The influences of track curve radius and super elevation on nonlinear critical speed were investigated.

In recent years, with the needs for fast and comfortable travel, the convenient high-speed railway train is more and more popular. With the rapid development of high-speed railway, the running speed of trains becomes faster and faster. The maximum running speed of trains being in service continuously sets new record. The Chinese CRH380A set the record of 486.1 km/h in December 3, 2010. Besides the notable increase of the top speed, the sustainable operation speed is also continually boosted. For example, the commercial speed of Chinese CRH trains running on Beijing-Shanghai high-speed railway can keep a constant operating speed of 350 km/h for long time. Because aerodynamic loads is proportional to the square of speed, the aerodynamic loads due to reverse air flow and cross wind for high-speed situation are much larger than that for low speed, so the effects of aerodynamic loads have to be considered. There have been some investigations on aerodynamic actions on railway vehcile in some respects [32–40]. These works, however, mostly concerned with seeking characteristics of flow fields or analyzing the forced vibration of vehicle by considering aerodynamic loads as external excitations. It seems that there are few works on the hunting stability of railway vehicles considering the effects of aerodynamic loads. The hunting motion of railway vehicles is a problem of self-excited vibration, whose mechanical mechanism is different from forced vibration. The results for forced vibration analysis can hardly be used to illustrate the characteristics of the self-excited vibration. Zeng and Lai [41] have studied the linear hunting stability and calculated the linear critical speed considering the influences of aerodynamic loads. The nonlinear critical speed, however, was not investigated there.

Therefore, the hunting stability study of high-speed railway vehicle considering the influences of aerodynamic loads is still a problem deserving further investigations, even for the situation of running in open air. For dynamical system of railway vehicles, the suspension is a very important subsystem affecting critical speed, and the dependence of critical speed on suspension parameters is an important problem worthy of study. Although there were some investigations for the situation without aerodynamic loads, there are hardly any studies on this problem incorporating the influences of aerodynamic loads.

The dependence of linear and nonlinear critical speed on suspension parameter, incorporating the influences of aerodynamic loads, was investigated in this study. The variation trends of critical speed versus suspension parameters were obtained; the dominant suspension parameters were identified. There are many suspension parameters affecting linear and nonlinear critical speeds, so it becomes a problem of multi-factorial experiment. In order to investigate quickly and effectively the variation trends of critical speed versus

suspension parameters, identify the dominant suspension parameter incorporating the influences of aerodynamic loads, the orthogonal test method was employed.

In Sect. 2, a mathematical model developed in this study capable of incorporating influences of aerodynamic loads is shown. A mechanism explaining the differences of hunting behavior between two situations with or without effects of aerodynamic loads is shown in Sects. 3 and 4, where the changes of wheel/rail contact forces due to aerodynamic loads play a major role. A computer program capable of incorporating influences of aerodynamic loads was written, with which the linear and nonlinear critical speeds were calculated. The orthogonal test method was employed to investigate the dependence of linear and nonlinear critical speeds on suspension parameters with high efficiency. The critical speeds for three situations—one without considering aerodynamic loads, the other two considering the influences of reverse airflow and cross wind with different velocities—are calculated respectively. The variation trends of linear and nonlinear critical speeds versus suspension parameters (considering aerodynamic loads) were obtained and compared; the dominant suspension parameters were identified. Details for procedure and numerical results are given in Sects. 5 and 6. The last section is conclusion, focusing on some key points of this paper.

2 A mathematical model for dynamical system of railway vehicles incorporating the influences of aerodynamic loads

The mathematical model for dynamical system of a high-speed railway vehicle with 23 degrees of freedom (DOFs) was set up considering the influences of aerodynamic loads. These 23 DOFs are lateral displacements and yaw angles (y_w and ψ_w) of four wheel-sets; lateral and vertical displacements (y_t and z_t), yaw, roll, and pitch angles (ψ_t, ϕ_t, and β_t) of two bogie frames; lateral and vertical displacements (y_c and z_c), yaw, roll, and pitch angles (ψ_c, ϕ_c, and β_c) of car body. They can be expressed as $\boldsymbol{Y}_1$. The roll angle ϕ_w and vertical displacement z_w of wheel-set are not independent, being subject to wheel/rail geometric constraints.

$$\boldsymbol{Y}_1 = [y_{w1}\ y_{w2}\ y_{w3}\ y_{w4}\ \psi_{w1}\ \psi_{w2}\ \psi_{w3}\ \psi_{w4}\ y_{t1}\ z_{t1}\ \phi_{t1}\ \psi_{t1}\ \beta_{t1}\ y_{t2}\ z_{t2}\ \phi_{t2}\ \psi_{t2}\ \beta_{t2}\ y_c\ z_c\ \phi_c\ \psi_c\ \beta_c]^{\mathrm{T}}. \quad (1)$$

In addition, there are lateral displacements y_h of spring-damping connecting point of two lateral dampers and longitudinal displacements y_s of spring-damping connecting point of four yaw dampers. They can be expressed as $\boldsymbol{Y}_2$.

$$\boldsymbol{Y}_2 = [y_{hL}\ y_{hR}\ y_{sL1}\ y_{sR1}\ y_{sL2}\ y_{sR2}]^{\mathrm{T}}. \quad (2)$$

The railway vehicle dynamical system is shown in Fig. 1, where stiffness and damping elements have been incorporated into the suspensions. The equations of motions for the dynamical system of a railway vehicle considering the influences of aerodynamic loads can be expressed as follows.

$$\begin{bmatrix} \boldsymbol{M}_1 & 0 \\ 0 & 0 \end{bmatrix} \begin{Bmatrix} \ddot{\boldsymbol{Y}}_1 \\ \ddot{\boldsymbol{Y}}_2 \end{Bmatrix} + \begin{bmatrix} \boldsymbol{C}_1(\boldsymbol{P}_f, \boldsymbol{U}, \boldsymbol{V}, \boldsymbol{Y}, \dot{\boldsymbol{Y}}) & 0 \\ \boldsymbol{C}_2 & \boldsymbol{C}_3 \end{bmatrix} \begin{Bmatrix} \dot{\boldsymbol{Y}}_1 \\ \dot{\boldsymbol{Y}}_2 \end{Bmatrix} + \begin{bmatrix} \boldsymbol{K}_1(\boldsymbol{P}_f, \boldsymbol{U}, \boldsymbol{V}, \boldsymbol{Y}, \dot{\boldsymbol{Y}}) & \boldsymbol{K}_2 \\ \boldsymbol{K}_3 & \boldsymbol{K}_4 \end{bmatrix} \begin{Bmatrix} \boldsymbol{Y}_1 \\ \boldsymbol{Y}_2 \end{Bmatrix} = \boldsymbol{P}_f(C_L, C_C, C_{Mx}, C_{My}, C_{Mz}, \boldsymbol{U}, \boldsymbol{V}), \quad (3)$$

where C_L, C_C, M_X, M_Y, and M_Z are the coefficient of aerodynamic lift force, lateral force, overturning moment, pitch moment and yaw moment, respectively; $\boldsymbol{U}$ and $\boldsymbol{V}$ are the velocity of crosswind and the running speed of vehicle, respectively; $\boldsymbol{M}_1$ is the inertia matrix, $\boldsymbol{P}_f$ the vector of aerodynamic force; $\boldsymbol{C}_1(\boldsymbol{P}_f, \boldsymbol{U}, \boldsymbol{V}, \boldsymbol{Y}, \dot{\boldsymbol{Y}})$, $\boldsymbol{K}_1(\boldsymbol{P}_f, \boldsymbol{U}, \boldsymbol{V}, \boldsymbol{Y}, \dot{\boldsymbol{Y}})$ are the damping matrix and stiffness matrix, respectively, some elements of $\boldsymbol{C}_1$ and $\boldsymbol{K}_1$ are affected by the aerodynamic loads. Such effects of aerodynamic loads on damping and stiffness matrix are not taken into account in other previous studies. It is obvious that the dynamical system of railway vehicle considering the influences of aerodynamic loads is much different from that without aerodynamic loads. The details of these influences are presented in Sect. 4.

With the increase of the running speed, the influences of aerodynamic loads on $\boldsymbol{C}_1$ and $\boldsymbol{K}_1$ become more and more obvious. Most studies, however, did not take such influences into account. For this reason, a computational program capable of incorporating them was written in this study, by using which the dependences of critical speeds on suspension parameters were calculated numerically.

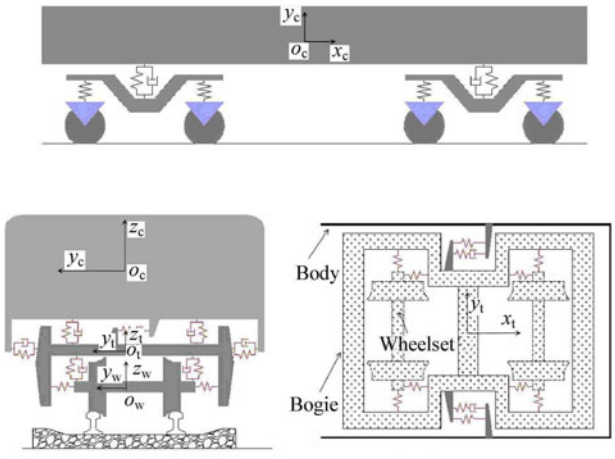

Fig. 1 The sketch of the railway vehicle dynamical system

3 Nonlinear factors

There are many nonlinear factors in dynamical system of railway vehicles such as nonlinear wheel/rail geometric constraints (wheel/rail contact nonlinearity), nonlinear creep force and nonlinear suspension system etc. In this study, nonlinear wheel/rail geometric constraints and nonlinear creep force were considered.

3.1 Nonlinear wheel/rail geometric constraints (wheel/rail contact nonlinearity)

The profiles of wheel/rail are composed of several curves, and the wheel/rail contact relationship includes wheel-set rolling radius, contact angle, roll angle of wheel-set, transverse radius of wheel profile and transverse radius of rail profile etc. It can be considered as nonlinear functions of wheel-set lateral displacement y_w. Because of the difficulty to express those contact parameters as explicit functions of y_w, the profiles of wheel and rail are described as discrete point set in terms of y_w. The contact parameters are calculated by using spline interpolation. With the obtained contact parameters, the wheel/rail normal contact forces and creep forces can then be calculated.

The nonlinear wheel/rail geometric constraint is the most important nonlinear factor in dynamical system of railway vehicle. In this study, the LMA/UIC60 wheel/rail pair is adopted.

3.2 Nonlinear creep force

According to Kalker's linear creep theory, the creep coefficients are written as

$$\begin{aligned}
f_{11i} &= Gmn\left[\frac{3\pi(1-\sigma^2)}{2E(A+B)}N_i(\boldsymbol{P}_f,\boldsymbol{U},\boldsymbol{V},\boldsymbol{Y},\dot{\boldsymbol{Y}},\ddot{\boldsymbol{Y}})\right]^{\frac{2}{3}}C_{11},\\
f_{22i} &= Gmn\left[\frac{3\pi(1-\sigma^2)}{2E(A+B)}N_i(\boldsymbol{P}_f,\boldsymbol{U},\boldsymbol{V},\boldsymbol{Y},\dot{\boldsymbol{Y}},\ddot{\boldsymbol{Y}})\right]^{\frac{2}{3}}C_{22},\\
f_{23i} &= Gmn\left[\frac{3\pi(1-\sigma^2)}{2E(A+B)}N_i(\boldsymbol{P}_f,\boldsymbol{U},\boldsymbol{V},\boldsymbol{Y},\dot{\boldsymbol{Y}},\ddot{\boldsymbol{Y}})\right]C_{23},\\
f_{33i} &= Gmn\left[\frac{3\pi(1-\sigma^2)}{2E(A+B)}N_i(\boldsymbol{P}_f,\boldsymbol{U},\boldsymbol{V},\boldsymbol{Y},\dot{\boldsymbol{Y}},\ddot{\boldsymbol{Y}})\right]^{\frac{4}{3}}C_{33},\\
(A+B) &= \frac{1}{2}\left(\frac{1}{R_w}+\frac{1}{r_r}+\frac{1}{r_w}\right),
\end{aligned} \tag{4}$$

where R_w, r_w, r_r, G, C_{ij}, σ, m, n are the wheel-set rolling radius, transverse radius of wheel profile, transverse radius of rail profile, the shear modulus, non-dimension Kalker coefficient, poisson ratio and coefficients related to A and B, respectively.

$N_i(\boldsymbol{P}_f,\boldsymbol{U},\boldsymbol{V},\boldsymbol{Y},\dot{\boldsymbol{Y}},\ddot{\boldsymbol{Y}})$ denotes the wheel/rail normal force which is affected by aerodynamic loads and the motions of vehicle system. The creep forces and moments are calculated by Eq. (5), where F_{xi} is the longitudinal creep force, and F_{yi} the lateral creep force.

$$\begin{aligned}
F_{xi} &= -f_{11i}\gamma_{xi},\\
F_{yi} &= -f_{22i}\gamma_{yi} - f_{23i}\gamma_{si},\\
M_{zi} &= f_{23i}\gamma_{yi} - f_{33i}\gamma_{si}.
\end{aligned} \tag{5}$$

In order to evaluate the wheel/rail creep forces more accurately, modifications for the creep forces in Eq. (5) can be made according to nonlinear creep force model (see, e.g., Ref. [42])

$$F_i = \sqrt{F_{xi}^2 + F_{yi}^2}, \tag{6}$$

$$F_i' = \begin{cases} fN_{iF}\left[\dfrac{F_i}{fN_{iF}} - \dfrac{1}{3}\left(\dfrac{F_i}{fN_{iF}}\right)^2 + \dfrac{1}{27}\left(\dfrac{F_i}{fN_{iF}}\right)^3\right], \\ \qquad F_i \leqslant 3fN_{iF}, \\ fN_{iF}, \quad F_i > 3fN_{iF}, \end{cases} \tag{7}$$

where $N_{iF} = N_i(\boldsymbol{P}_f,\boldsymbol{U},\boldsymbol{V},\boldsymbol{Y},\dot{\boldsymbol{Y}},\ddot{\boldsymbol{Y}})$, f is the friction coefficient. Saturation constant ε is calculated by Eq. (8).

$$\varepsilon = \frac{F_i'}{F_i}. \tag{8}$$

Substituting Eqs. (4)–(5) and (8) into Eq. (9), the modified creep forces and moments are obtained as

$$\begin{aligned}
F_{xi}' &= \varepsilon F_{xi},\\
F_{yi}' &= \varepsilon F_{yi},\\
M_{zi}' &= \varepsilon M_{zi}.
\end{aligned} \tag{9}$$

4 Influences of aerodynamic loads on the dynamical system of railway vehicles

Distributed normal pressure and shear stress on the vehicle body surface induced by air flow can form the resultant forces/moments (F_i (i = 1, 2, 3), M_i (i = 1, 2, 3)) known as aerodynamic drag force, lateral force and lift force in respectively the longitudinal, lateral and vertical directions, and the overturning moment about x-axis, the pitch moment about y-axis, the yaw moment about z-axis. They are expressed as

$$\begin{aligned}
F_i &= \frac{1}{2}\rho A C_i|\boldsymbol{V}+\boldsymbol{U}|^2, \quad i = 1,2,3,\\
C_1 &= C_D, \quad C_2 = C_L, \quad C_3 = C_C,\\
M_i &= \frac{1}{2}\rho A L C_{Mi}|\boldsymbol{V}+\boldsymbol{U}|^2, \quad i = 1,2,3,\\
C_{M1} &= C_{Mx}, \quad C_{M2} = C_{My}, \quad C_{M3} = C_{Mz},
\end{aligned} \tag{10}$$

F_i and M_i are the components of the vector $\boldsymbol{P}_f$ in Eq. (3), which can be written as

$$\boldsymbol{P}_f = [F_1 \;\; F_2 \;\; F_3 \;\; M_1 \;\; M_2 \;\; M_3]^T.$$

These components of aerodynamic loads make the axle loads and normal contact forces changed, and then change the creep forces and gravitational restoring forces. In addition, the position of vehicle dynamical system can be also changed, which make the points of contact (and consequently the contact relations) between the wheel and the rail different from the ones without actions of aerodynamic loads. Because of these influences of aerodynamic loads, the hunting stability of high-speed railway vehicles certainly changes. In this study, the steady aerodynamic loads were considered.

4.1 Influences of aerodynamic loads on wheel/rail normal force and gravitational restoring force

The aerodynamic loads have obvious effect on the wheel/rail normal forces. The positive aerodynamic lift force can re-

duce the axle load; the aerodynamic lateral force and overturning moment about x-axis can cause the differences of the normal forces between left wheel and right wheel; the pitch moment about y-axis can cause the differences of the normal forces between front wheel and rear wheel. The normal forces can be obtained by the motion equations of roll angle ϕ_w and vertical displacement z_w of wheel-set (ϕ_w and z_w are subject to wheel/rail geometric constraint, not independent), as shown in Eq. (11).

$$\begin{aligned} N_L &= 2\cos\alpha_L(W + M_w\ddot{z}_w - F_{pzL} - F_{pzR} - f_{pzL} - f_{pzR}) \\ &\quad + \frac{2\cos\alpha_L}{d_0}[I_{wx}\ddot{\phi}_w - d_{zx}F_{pzL} + d_{zx}F_{pzR} - d_{zx}f_{pzL} \\ &\quad + d_{zx}f_{pzR} - F_{yL}R_L - F_{yR}R_R - R_R N_R \sin(\alpha_R - \phi_w) \\ &\quad + R_L N_L \sin(\alpha_L + \phi_w)], \\ N_R &= 2\cos\alpha_R(W + M_w\ddot{z}_w - F_{pzL} - F_{pzR} - f_{pzL} - f_{pzR}) \\ &\quad - \frac{2\cos\alpha_R}{d_0}[I_{wx}\ddot{\phi}_w - d_{zx}F_{pzL} + d_{zx}F_{pzR} - d_{zx}f_{pzL} \\ &\quad + d_{zx}f_{pzR} - F_{yL}R_L - F_{yR}R_R - R_R N_R \sin(\alpha_R - \phi_w) \\ &\quad + R_L N_L \sin(\alpha_L + \phi_w)], \end{aligned} \tag{11}$$

where subscript L and R represent left and right respectively, N_L and N_R are normal contact force, α_L and α_R the contact angles, R_L and R_R the wheel rolling radii, d_{zx} is half of lateral distance of axle box, d_0 the half of track gauge, F_{pzL}, F_{pzR}, f_{pzL}, and f_{pzR} are the variation of suspension stiffness force and damping force of primary suspension, F_{yL} and F_{yR} the lateral creep forces, respectively.

N_L and N_R are actually related to aerodynamic loads. It is because that most terms on the right hand side of Eq. (11) are implicitly related to aerodynamic loads. The geometric parameters (α_L, α_R, R_L, R_R, etc.) at the points of wheel/rail contact are determined by the position of the vehicle system, which is affected by aerodynamic loads. The vertical displacements and roll angles are subject to wheel/rail geometric constraints, which are also affected by aerodynamic loads because the geometric constraints are determined by the points of contact. The spring forces of suspension system are also affected by aerodynamic loads. F_{pzL} and F_{pzR} of the first wheel-set are taken for example to explain in detail the effects induced by aerodynamic loads. If the aerodynamic loads are not considered, they can be expressed as

$$\begin{aligned} F_{pzL} &= K_{pz}(d_{zx}\phi_t - l_t\beta_t), \\ F_{pzR} &= K_{pz}(-d_{zx}\phi_t + l_t\beta_t), \end{aligned} \tag{12}$$

where K_{pz} is vertical stiffness of primary suspension, ϕ_t and β_t are roll angle and pitch angle of frame respectively, d_{zx} half of lateral distance of axle box, and l_t is half of longitudinal distance of axle box. After considering the actions of aerodynamic loads, F_{pzL} and F_{pzR} can be written as

$$\begin{aligned} F_{pzL} &= K_{pz}[d_{zx}\phi_t(C_L, C_C, C_{Mx}, C_{My}, C_{Mz}, \boldsymbol{U}, \boldsymbol{V}) \\ &\quad - l_t\beta_t(C_L, C_C, C_{Mx}, C_{My}, C_{Mz}, \boldsymbol{U}, \boldsymbol{V})], \\ F_{pzR} &= K_{pz}[-d_{zx}\phi_t(C_L, C_C, C_{Mx}, C_{My}, C_{Mz}, \boldsymbol{U}, \boldsymbol{V}) \\ &\quad + l_t\beta_t(C_L, C_C, C_{Mx}, C_{My}, C_{Mz}, \boldsymbol{U}, \boldsymbol{V})]. \end{aligned} \tag{13}$$

Therefore N_L and N_R are functions of aerodynamic loads, and can be written as

$$N_L = N_L(\boldsymbol{P}_f, \boldsymbol{U}, \boldsymbol{V}, \boldsymbol{Y}, \dot{\boldsymbol{Y}}, \ddot{\boldsymbol{Y}}),$$

$$N_R = N_R(\boldsymbol{P}_f, \boldsymbol{U}, \boldsymbol{V}, \boldsymbol{Y}, \dot{\boldsymbol{Y}}, \ddot{\boldsymbol{Y}}),$$

where $\boldsymbol{Y}$, $\dot{\boldsymbol{Y}}$, $\ddot{\boldsymbol{Y}}$ are also functions of aerodynamic loads.

The gravitational restoring force can subsequently be obtained in terms of normal contact force, roll angle of wheel-set and contact angle, as shown in Eq. (14). It is thus obvious that aerodynamic loads can change the gravitational restoring force, which can be written as

$$\begin{aligned} F_{\text{restoring}} &= N_L(\boldsymbol{P}_f, \boldsymbol{U}, \boldsymbol{V}, \boldsymbol{Y}, \dot{\boldsymbol{Y}}, \ddot{\boldsymbol{Y}})\sin(\alpha_L + \phi_w) \\ &\quad - N_R(\boldsymbol{P}_f, \boldsymbol{U}, \boldsymbol{V}, \boldsymbol{Y}, \dot{\boldsymbol{Y}}, \ddot{\boldsymbol{Y}})\sin(\alpha_R - \phi_w), \end{aligned} \tag{14}$$

where α_L, α_R, ϕ_w are also functions of aerodynamic loads.

4.2 Influences of aerodynamic loads on creep forces and moments

It is seen from Eqs. (4) and (8) that the creep coefficients and saturation constant ε are both the functions of wheel/rail normal contact force $N_i = N_i(\boldsymbol{P}_f, \boldsymbol{U}, \boldsymbol{V}, \boldsymbol{Y}, \dot{\boldsymbol{Y}}, \ddot{\boldsymbol{Y}})$. As shown in Eq. (11), the aerodynamic loads can change the normal contact forces. In addition, the positions of wheel-set change under the actions of aerodynamic loads, so the wheel/rail contact parameters (R_w, r_w, r_r etc.) are also changed. Thus the creep coefficients are evidently changed, as shown in Eq. (4), due to the presence of aerodynamic loads. Similarly, saturation constant ε is changed by the aerodynamic loads as shown in Eqs. (6)–(8). Therefore, it is apparent that aerodynamic loads can change the creep forces and moments.

These changes of restoring forces and creep forces (moments) induced by aerodynamic loads are manifested in the stiffness matrix and damping matrix of Eq. (3), which indicate that the intrinsic characteristics of dynamical system of high-speed railway vehicles are changed. And then it is clear that the influences of aerodynamic loads on the vehicle system are fundamental and intricate, not only acting as the external excitations.

5 Determination of linear and nonlinear critical speeds

To analyze the linear hunting stability of railway vehicle system, the linearization of the nonlinear dynamic equations of vehicle system is performed at the equilibrium position. In order to evaluate the equilibrium position of vehicle system under steady aerodynamic loads, one can set $\dot{\boldsymbol{Y}} = \dot{\boldsymbol{Y}} = \boldsymbol{0}$ in Eq. (3), and then a set of nonlinear algebraic equations are obtained. The equilibrium position $\boldsymbol{Y} = \boldsymbol{Y}_0$ is obtained by solving the nonlinear algebraic equations by using Newton

iteration. The linearized equations at the equilibrium position can be written as Eq. (15).

$$\begin{bmatrix} \boldsymbol{M}_1 & 0 \\ 0 & 0 \end{bmatrix} \begin{Bmatrix} \ddot{\boldsymbol{Y}}_1 \\ \ddot{\boldsymbol{Y}}_2 \end{Bmatrix} + \begin{bmatrix} \boldsymbol{C}_1(\boldsymbol{P}_\mathrm{f}, \boldsymbol{U}, \boldsymbol{V}, \boldsymbol{Y}, \dot{\boldsymbol{Y}}) & 0 \\ \boldsymbol{C}_2 & \boldsymbol{C}_3 \end{bmatrix}\Bigg|_{\boldsymbol{Y}=\boldsymbol{Y}_0} \begin{Bmatrix} \dot{\boldsymbol{Y}}_1 \\ \dot{\boldsymbol{Y}}_2 \end{Bmatrix} + \begin{bmatrix} \boldsymbol{K}_1(\boldsymbol{P}_\mathrm{f}, \boldsymbol{U}, \boldsymbol{V}, \boldsymbol{Y}, \dot{\boldsymbol{Y}}) & \boldsymbol{K}_2 \\ \boldsymbol{K}_3 & \boldsymbol{K}_4 \end{bmatrix}\Bigg|_{\boldsymbol{Y}=\boldsymbol{Y}_0} \begin{Bmatrix} \boldsymbol{Y}_1 \\ \boldsymbol{Y}_2 \end{Bmatrix} = \boldsymbol{0}. \tag{15}$$

Equation (16) is the reduced order equation, where $\boldsymbol{x} = (\boldsymbol{0}, \boldsymbol{Y}_0)$ represents the equilibrium position.

$$\dot{\boldsymbol{x}} = \boldsymbol{A}\boldsymbol{x}, \quad \boldsymbol{A} = \left[\frac{\partial f_i}{\partial x_j}\right]\Bigg|_{\boldsymbol{x}=(\boldsymbol{0},\boldsymbol{Y}_0)}, \quad i, j = 1, 2, \cdots, 52. \tag{16}$$

As is well known, the stability of nonlinear dynamical system described by Eq. (3) in the neighbourhood of its equilibrium point can be determined by the eigenvalues of Jacobian matrix $\boldsymbol{A}$. If all the eigenvalues have negative real parts, the system is asymptotically stable. If there is at least one eigenvalue with positive real part, the system is unstable. When the maximum real part turns to be zero, the vehicle system comes to a critical state, and the corresponding speed is the linear critical speed, as seen in Fig. 2.

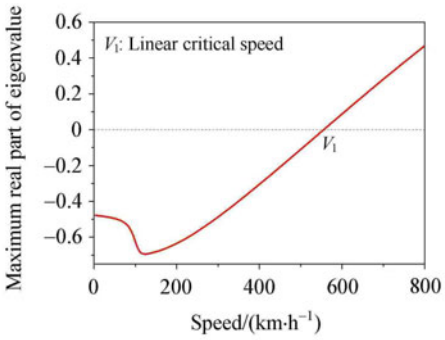

Fig. 2 A schematic diagram of linear critical speed

As for the dynamical system of railway vehicle with subcritical bifurcation, the nonlinear critical speed should be the smallest bifurcation point V_n, as shown in Fig. 3. There will be three coexisting attractors in the speed region between V_c (above which the zero solution is unstable) and V_n, two of which are stable and the other one is unstable. An appropriate way to determine the smallest bifurcation point is to apply the method known as path following. During the process of calculating the nonlinear critical speed by using path following method, a periodic solution for a slightly greater running speed is taken as the initial value and numerical time integration procedure is adopted to solve the nonlinear differential equations. At a certain speed, the initial-value problem of the nonlinear system tends to a stable zero solution. This speed is the smallest bifurcation point which corresponds to the nonlinear critical speed.

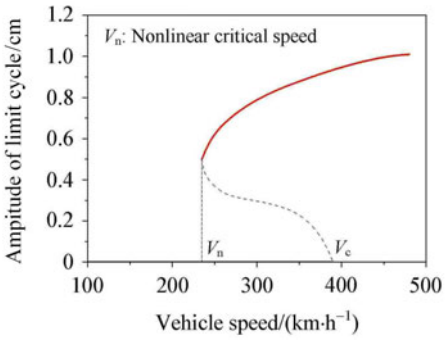

Fig. 3 A schematic diagram of nonlinear critical speed

6 Results and discussions for linear and nonlinear critical speed considering influences of steady aerodynamic loads in open air

Based on the theoretical analysis above, a computer program capable of incorporating effects of aerodynamic loads was developed, by using which the linear and nonlinear critical speeds can be calculated numerically. The program had been verified before further analysis is performed. Some verification was shown in Ref. [41].

There are many suspension parameters that can affect the critical speed, such as longitudinal, lateral and vertical stiffness of primary and secondary suspension systems; primary vertical damping; damping of lateral and yaw dampers; stiffness of spring-damping connecting point of lateral and yaw dampers etc. Various combinations of these parameters can lead to different critical speed. If calculations are performed for every parameter combination, the costs will be unacceptable. Therefore, the orthogonal test method is introduced in this study, which would improve the efficiency. In this section, the variation trends of critical speeds with suspension parameters are investigated and the dominant suspension parameters are identified.

The orthogonal table should be determined firstly, i.e. the tests to be done have to be selected among the complete set. 8 factors are selected, and each factor has 7 levels. Then the orthogonal table L_{49} (8^7) is adopted, as shown in Table 2 (Appendix). The selected 8 factors and their levels are shown in Table 1. According to the arrangement of factors in Table 2 (Appendix), the linear and nonlinear critical speeds are calculated for three situations (A, B, C): one without effects of aerodynamic loads, the other two considering the effects of aerodynamic loads induced by the reverse air flow and the crosswind with different velocities. The numerical results are also shown in Table 2 (Appendix). Details and discussions for linear and nonlinear hunting stability are respectively presented in Subsects. 6.1 and 6.2.

It is necessary to note that the aerodynamic coefficients adopted in this study are provided by the aerodynamic research group directed by Professor Guowei Yang at Institute of Mechanics, Chinese Academy of Sciences. The aerodynamic coefficients are those for the third vehicle of a train set with six vehicles.

Table 1 Selection of suspension parameters

	Suspension parameters	Level 1	Level 2	Level 3	Level 4	Level 5	Level 6	Level 7
Factor 1	Primary longitudinal stiffness/(N·m^{-1})	11 234 000	12 056 000	12 878 000	13 700 000	14 522 000	15 344 000	16 166 000
Factor 2	Primary lateral stiffness/(N·m^{-1})	4 501 800	4 831 200	5 160 600	5 490 000	5 819 400	6 148 800	6 478 200
Factor 3	Stiffness of spring-damping connecting point of yaw damper/(N·m^{-1})	7 232 400	7 761 600	8 290 800	8 820 000	9 349 200	9 878 400	10 407 600
Factor 4	Damping of yaw damper/(N·s·m^{-1})	200 900	215 600	230 300	245 000	259 700	274 400	289 100
Factor 5	Stiffness of spring-damping connecting point of lateral damper/(N·m^{-1})	28 126 000	30 184 000	32 242 000	34 300 000	36 358 000	38 416 000	40 474 000
Factor 6	Damping of lateral damper/(N·s·m^{-1})	96 432	103 488	110 544	117 600	124 656	131 712	138 768
Factor 7	Secondary lateral and longitudinal stiffness/(N·m^{-1})	130 954	140 536	150 118	159 700	169 282	178 864	188 446
Factor 8	Secondary vertical stiffness/(N·m^{-1})	812 456	871 904	931 352	990 800	1 050 248	1 109 696	1 169 144

6.1 Linear hunting stability

It is seen from the numerical results of linear critical speeds in Table 2 (Appendix), for all 49 cases, the linear critical speeds incorporating the influences of aerodynamic loads are always smaller than the ones without aerodynamic loads. As the velocity of crosswind increase from 5.4 m/s to 10.7 m/s, the linear critical speed decrease. The root locus diagram for three aerodynamic situations are shown in Fig. 4, which shows the loci of the eigenvalues as the running speeds of vehicles increase beyond the critical speed. It is obvious that aerodynamic loads significantly change the variation trends of root loci. Yellow, green and wine lines in Fig. 4 are lines connecting points with zero real parts in different aerodynamic situations. These lines show that the values of imaginary parts of eigenvalues corresponding to instability (indicating the oscillation frequency) decrease as the velocity of crosswind increases, for any damping of lateral damper. The real parts of eigenvalues considering aerodynamic loads are larger than the ones without aerodynamic loads for any running speed. This means that the effective damping of dynamical system of vehicles becomes weaker and be more prone to hunting after consideration of aerodynamic loads. That is to say, aerodynamic loads would deteriorate the hunting stability of railway vehicles. Such effects become more evident as the velocity of crosswind increases. It also can be seen that the differences between eigenvalues corresponding to different aerodynamic situations are small when the running speed is low, but obvious when the vehicle speed is high. This justifies the consideration of aerodynamic loads for high-speed railway vehicles and the neglect of them for low-speed ones.

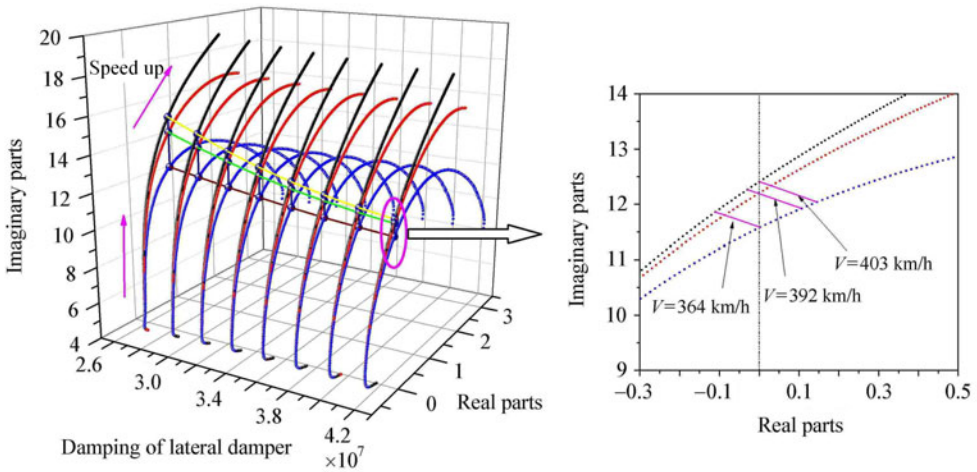

Fig. 4 Root locus diagram of the eigenvalue corresponding to instability mode for three aerodynamic situations (black lines: situation without aerodynamic loads; red lines: situation with aerodynamic loads, the velocity of crosswind being 5.4 m/s; blue lines: situation with aerodynamic loads, the velocity of crosswind being 10.7 m/s)

The results of range analysis for the linear critical speed in Table 2 (Appendix) are shown in Fig. 5. It is seen that, for all aerodynamic situations, the most dominant factor affecting linear critical speed is factor 4 (the damping of yaw damper), the effects of factor 1 (the primary longitudinal stiffness) and 6 (the damping of lateral damper) are also obvious. The range becomes smaller after considering the aerodynamic loads. That is to say, the changes of linear critical speed due to the variations of suspension parameter become smaller. This means that the influences of aerodynamic loads decrease the sensitivity of linear critical speed to suspension parameters. Such effects become more evident as the velocity of crosswind increases.

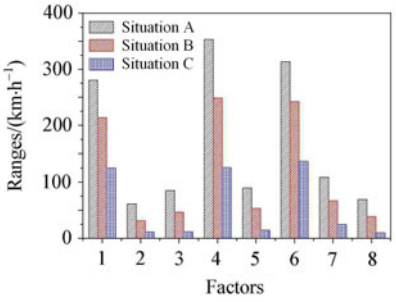

Fig. 5 The range analysis of the linear critical speed (A: situation without aerodynamic loads; B: situation with aerodynamic loads, the velocity of crosswind being 5.4 m/s; C: situation with aerodynamic loads, the velocity of crosswind being 10.7 m/s)

In view of the significance of the impact of primary longitudinal stiffness, damping of yaw damper and damping of lateral damper on linear critical speed, the dependences of average linear critical speed on these three parameters were investigated and shown in Figs. 6–8. The average linear critical speed is the average value of the results for tests, a factor of which has the same level in the orthogonal table. For example, point *P* in Fig. 6 denote the mean of the linear critical speed (for situation C) of all seven tests, factor 1 of which has the same level—"1". It is seen from these three figures that, for the value range considered, the linear critical speed decreases with the rise of primary longitudinal stiffness or damping of lateral damper, and increases with the rise of damping of yaw damper. In addition, the curves of the linear critical speed versus the suspension parameters for these three aerodynamic situations are not parallel. This means that joint effects of aerodynamic loads and these three suspension parameters also affect the linear critical speed. The differences between linear critical speeds corresponding to different aerodynamic situations decreases with the rise of primary longitudinal stiffness or damping of lateral damper, and increases with the rise of damping of yaw damper.

6.2 Nonlinear hunting stability

Similar investigations were conducted for nonlinear critical speeds shown in Table 2 (Appendix). The results were also compared with the linear ones.

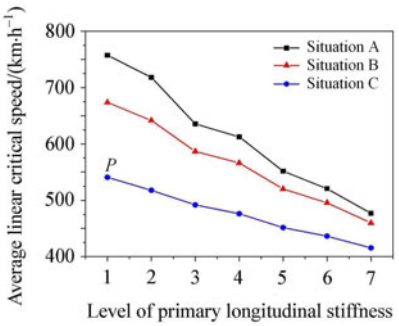

Fig. 6 The dependence of average linear critical speed on primary longitudinal stiffness (A: situation without aerodynamic loads; B: situation with aerodynamic loads, the velocity of crosswind being 5.4 m/s; C: situation with aerodynamic loads, the velocity of crosswind being 10.7 m/s)

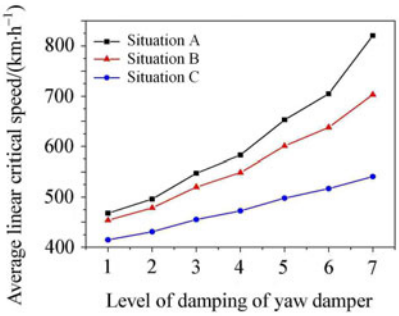

Fig. 7 The dependence of average linear critical speed on damping of yaw damper

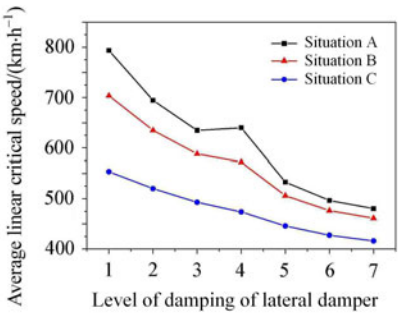

Fig. 8 The dependence of average linear critical speed on damping of lateral damper

As shown in Table 2 (Appendix), the nonlinear critical speeds for situations considering the influences of aerodynamic loads (situations B and C) are not always smaller than the ones without aerodynamic loads (situation A). For situation C (the velocity of crosswind being 10.7 m/s), the nonlinear critical speeds are always smaller than that of situation A; whereas for situation B (the velocity of crosswind being 5.4 m/s), the nonlinear critical speeds are close to or even greater than (for particular cases) that of situation A, as shown in Fig. 9. This is different from the results of linear critical speed.

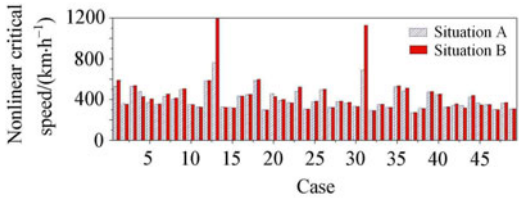

Fig. 9 The nonlinear critical speeds for situation A and B in Table 2 (Appendix)

The results of range analysis for the nonlinear critical speed in Table 2 (Appendix) are shown in Fig. 10, whose counterparts for linear case are shown in Fig. 5. Unlike the results in Fig. 5, the most dominant factor affecting nonlinear critical speed is factor 6 (the damping of lateral damper) instead. For situations A and C, three important factors affecting the nonlinear critical speed are the damping of lateral damper, primary longitudinal stiffness and damping of yaw damper. Whereas for situation B, in addition to these three parameters, the stiffness of spring-damping connecting point of lateral damper and yaw damper can also have obvious influence. For situation B, the ranges are larger than those of other two situations. This means that the nonlinear critical speeds are most sensitive to suspension parameters for situation B, which is also different from that of linear critical speed.

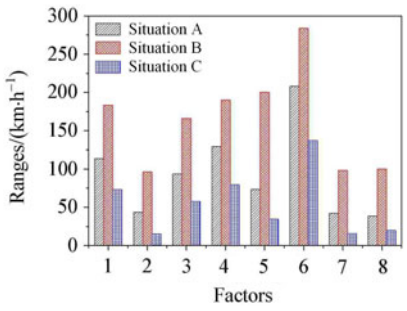

Fig. 10 The range analysis of the nonlinear critical speed

The dependence of average nonlinear critical speed on primary longitudinal stiffness, damping of yaw damper and damping of lateral damper are respectively shown in Figs. 11–13, being the counterparts for the linear case. As shown in these three figures, the variation curves of nonlinear critical speed with these three parameters are much different from the ones of linear critical speed. The nonlinear critical speeds for situation B are larger than or close to the nonlinear critical speeds for situation A and C. It is also seen from Figs. 11–13 that, for the value range considered, the nonlinear critical speed decreases undulately with the rise of primary longitudinal stiffness; decreases monotonously with the rise of damping of lateral damper; increases undulately with the rise of damping of yaw damper. The joint action of aerodynamic loads and these three suspension parameters also affect the nonlinear critical speed.

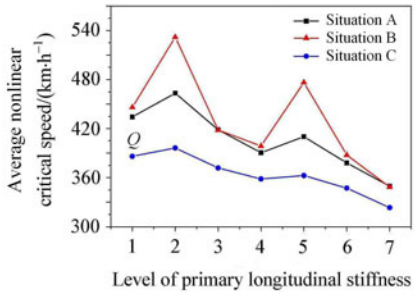

Fig. 11 The dependence of average nonlinear critical speed on primary longitudinal stiffness

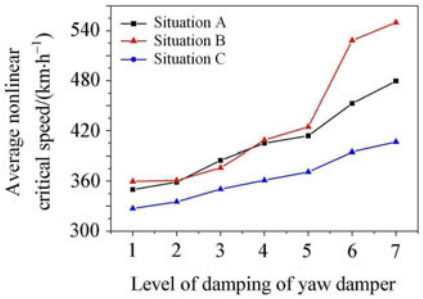

Fig. 12 The dependence of average nonlinear critical speed on damping of yaw damper

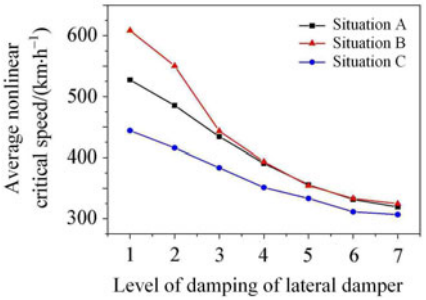

Fig. 13 The dependence of average nonlinear critical speed on damping of lateral damper

It is shown that the effects of aerodynamic loads on nonlinear critical speed are more complex than that on the linear one. The variation trends of nonlinear critical speeds for different aerodynamic situations seem to be short of definite direction of change (or may be in a complicated manner). Calculations of nonlinear critical speed for more aerodynamic situations are still of benefit.

It is seen that as the aerodynamic loads have complicated influences on the hunting stability of vehicles, it is very hard to obtain explicit mathematical expressions suitable for the direct quantitative explanation on the dominance of influential factors. A further examination is helpful.

7 Conclusions

The influences of steady aerodynamic loads, which are induced by reverse air flow and crosswind, on linear and non-

linear hunting stability of high-speed railway vehicles were studied. A mechanism is suggested to explain the change of hunting behavior due to actions of aerodynamic loads: the aerodynamic loads can change the position of dynamical system of vehicles (consequently the contact relations), the wheel/rail normal contact forces, and then the gravitational restoring forces/moments and the creep forces/moments. A mathematical model for hunting stability incorporating such influences was developed. Based on this model, a computer program capable of considering effects of aerodynamic loads was written, with which the linear and nonlinear critical speeds were calculated numerically. The orthogonal test method was employed to investigate the dependence of linear and nonlinear critical speeds on suspension parameters with high efficiency. The dominant factors affecting linear and nonlinear critical speeds were also identified on the basis of orthogonal test method. The consequences of the actions of aerodynamic loads on hunting stability can be summarized as follows:

For all three aerodynamic situations, the most dominant factor affecting the linear critical speed is damping of yaw damper, the effects of primary longitudinal stiffness and damping of lateral damper are also obvious. The influences of aerodynamic loads decrease the sensitivity of the linear critical speed to suspension parameters. Whether the aerodynamic loads are considered or not, the linear critical speed decreases with the rise of primary longitudinal stiffness and damping of lateral damper, but increases with the rise of damping of yaw damper.

The most dominant factor affecting nonlinear critical speed is the damping of lateral damper. The nonlinear critical speed decreases undulately with the rise of primary longitudinal stiffness, and decreases monotonously with damping of lateral damper. However, it increases undulately with damping of yaw damper. With the influences of aerodynamic loads considered, the linear critical speeds decrease with the rise of cross wind velocity, whereas it is not the case for the nonlinear critical speeds.

Combined actions of aerodynamic loads and suspension parameters do affect the linear and nonlinear critical speeds, in addition to exerting their influences independently.

Appendix Orthogonal table L_{49} (8^7) and the numerical results

Table 2 Orthogonal table L_{49} (8^7) and the numerical results for three situations: A: situation without aerodynamic loads; B: situation with aerodynamic loads, the velocity of crosswind being 5.4 m/s; C: situation with aerodynamic loads, the velocity of crosswind being 10.7 m/s

Cases	Factor 1	Factor 2	Factor 3	Factor 4	Factor 5	Factor 6	Factor 7	Factor 8	Linear critical speed/(km · h^{-1})			Nonlinearcritical speed/(km · h^{-1})		
									A	B	C	A	B	C
1	1	1	1	1	1	1	1	1	651	618	532.4	529	590	462
2	1	2	3	4	5	6	7	2	647	599	502.5	355	353	328
3	1	3	5	7	2	4	6	3	1 142	885	620	529	536	417
4	1	4	7	3	6	2	5	4	800	726.8	578	478	429	412
5	1	5	2	6	3	7	4	5	672	618	513.5	371	405	368
6	1	6	4	2	7	5	3	6	537	515	458	350	355	330
7	1	7	6	5	4	3	2	7	852	753.2	581	428	454	386
8	2	1	7	6	5	4	3	7	811	711	555.5	400	415	374
9	2	2	2	2	2	2	2	1	628	594.3	510.5	496	507	431
10	2	3	4	5	6	7	1	2	552	526	463.5	350	351	329
11	2	4	6	1	3	5	7	3	488	472	429.6	329	326	310
12	2	5	1	4	7	3	6	4	750	682	546	581	586	459
13	2	6	3	7	4	1	5	5	1 292	1 017	679.6	760	1 215	563
14	2	7	5	3	1	6	4	6	506	487.7	439	327	324	309
15	3	1	6	4	2	7	5	6	493.5	476	430	320	318	304
16	3	2	1	7	6	5	4	7	726	652	525	432	434	394
17	3	3	3	3	3	3	3	1	597	564	487.4	449	452	397
18	3	4	5	6	7	1	2	2	962	834.7	619.7	586	597	474
19	3	5	7	2	4	6	1	3	437	427	397.5	299	298	286
20	3	6	2	5	1	4	7	4	687	628.7	514.7	456	429	384
21	3	7	4	1	5	2	6	5	546	525	467.7	389	400	364

Table 2 Orthogonal table L_{49} (8^7) and the numerical results for three situations: A: situation without aerodynamic loads; B: situation with aerodynamic loads, the velocity of crosswind being 5.4 m/s; C: situation with aerodynamic loads, the velocity of crosswind being 10.7 m/s (continued)

Cases	Factor 1	Factor 2	Factor 3	Factor 4	Factor 5	Factor 6	Factor 7	Factor 8	Linear critical speed/(km · h^{-1})			Nonlinearcritical speed/(km · h^{-1})		
									A	B	C	A	B	C
22	4	1	5	2	6	3	7	5	543	519	457.6	370	369	354
23	4	2	7	5	3	1	6	6	871	770.5	588.6	479	522	430
24	4	3	2	1	7	6	5	7	405	398	374.4	308	307	295
25	4	4	4	4	4	4	4	1	560	532	465	377	385	351
26	4	5	6	7	1	2	3	2	909.7	785	587.6	496	501	422
27	4	6	1	3	5	7	2	3	421.7	413	386	324	324	306
28	4	7	3	6	2	5	1	4	577	545.7	473	380	383	351
29	5	1	4	7	3	6	2	4	553	524.8	459	362	374	338
30	5	2	6	3	7	4	1	5	472.7	458	418	331	332	315
31	5	3	1	6	4	2	7	6	813.5	716.6	553	690	1 129	519
32	5	4	3	2	1	7	6	7	391	385	363.8	291	292	281
33	5	5	5	5	5	5	5	1	524.8	501.6	444.6	349	352	328
34	5	6	7	1	2	3	4	2	445	434.4	402.5	322	322	306
35	5	7	2	4	6	1	3	3	661.7	619.5	520	526	534	451
36	6	1	3	5	7	2	4	3	649	602.4	502	485	513	425
37	6	2	5	1	4	7	3	4	361	356.6	341	271	272	263
38	6	3	7	4	1	5	2	5	451.3	439	403.5	312	313	299
39	6	4	2	7	5	3	1	6	653.3	602.8	501	469	478	415
40	6	5	4	3	2	1	7	7	607.7	574	491.5	446	453	392
41	6	6	6	6	6	6	6	1	494.5	475.8	427.6	322	328	308
42	6	7	1	2	3	4	5	2	427	417.4	388	341	357	329
43	7	1	2	3	4	5	6	2	427	417	387	340	318	322
44	7	2	4	6	1	3	5	3	602	562	475.8	419	441	368
45	7	3	6	2	5	1	4	4	510	492	442.5	366	348	336
46	7	4	1	5	2	6	3	5	433.3	422.4	391.4	349	350	316
47	7	5	3	1	6	4	2	6	380	374	355	302	301	290
48	7	6	5	4	3	2	1	7	514.8	494.7	441.3	363	372	336
49	7	7	7	7	7	7	7	1	470.3	455	414.6	308	310	296

References

1 Kim, P., Jung, J., Seok, J.: A parametric dynamic study on hunting stability of full dual-bogie railway vehicle. International Journal of Precision Engineering and Manufacturing **12**, 505–519 (2011)

2 Cheng, Y.C., Lee, S.Y.: Stability analysis of high-speed railway vehicle using half-car model. International Journal of Heavy Vehicle Systems **17**, 139–158 (2010)

3 Cheng, Y.C.: Hunting stability analysis of a railway vehicle system using a novel non-linear creep model. Proceedings of the Institution of Mechanical Engineers, Part F: Journal of Rail and Rapid Transit (2012)

4 Lee, S.Y., Cheng, Y.C.: Hunting stability analysis of high-speed railway vehicle trucks on tangent tracks. Journal of Sound and Vibration **282**, 881–898 (2005)

5 Hirotsu, T., Terada K., Hiraishi M., et al.: Simulation of hunting of rail vehicles: The case using a compound circular wheel protile. JSME International Journal, Series 3, Vibration, Control Engineering, Engineering for Industry **3**, 396–403 (1991)

6 Lee, S.Y., Cheng, Y.C.: Influences of the vertical and the roll motions of frames on the hunting stability of trucks moving on curved tracks. Journal of Sound and Vibration **294**, 441–453 (2006)

7 Cheng, Y.C., Lee, S.Y., Chen, H.H.: Modeling and nonlinear

hunting stability analysis of high-speed railway vehicle moving on curved tracks. Journal of Sound and Vibration **324**, 139–160 (2009)
8 Cheng, Y.C., Lee, S.Y.: Nonlinear analysis on hunting stability for high-speed railway vehicle trucks on curved tracks. Transactions of the ASME **127**, 324–332 (2005)
9 Liu, H.Y., Zeng, J., Lu, K.W.: A study of hopf bifurcation of hunting motion for high-speed passenger cars. Engineering Mechanics **22**, 224–228 (2005) (in Chinese)
10 Wang, F.C., Liao, M.K.: The lateral stability of train suspension systems employing inerters. Vehicle System Dynamics **48**, 619–643 (2010)
11 Dukkipati, R.V., Narayana Swamy, S.: Non-linear steady-state curving analysis of some unconventional rail trucks. Mechanism and Machine Theory **36**, 507–521 (2001)
12 Dukkipati, R.V., Narayana Swamy, S.: Lateral stability and steady state curving performance of unconventional rail trucks. Mechanism and Machine Theory **36**, 577–587 (2001)
13 True, H.: On the theory of nonlinear dynamics and its applications in vehicle systems dynamics. Vehicle System Dynamics **31**, 393-421 (1999)
14 Polach, O.: On non-linear methods of bogie stability assessment using computer simulations. Proceedings of the Institution of Mechanical Engineers, Part F: Journal of Rail and Rapid Transit **220**,13–27 (2006)
15 True, H.: Does a critical speed for railroad vehicles exist. Proceedings of the 1994 ASME/IEEE Joint (in Conjunction with Area 1994 Annual Technical Conference). IEEE, 125–131 (1994)
16 True, H., Kaas-Petersen, C.: A bifurcation analysis of nonlinear oscillations in railway vehicles. Vehicle System Dynamics **12**, 5–6 (1983)
17 True, H.: Multiple attractors and critical parameters and how to find them numerically: The right, the wrong and the gambling way. Vehicle System Dynamics **51**, 443–459 (2013)
18 True, H.: Railway vehicle chaos and asymmetric hunting. Vehicle System Dynamics **20**, 625–637 (1992)
19 Jensen, J.C., True, H.: Chaos and asymmetry in railway vehicle dynamics. Transportation Engineering **22**, 55–68 (1994)
20 Stichel, S.: Limit cycle behaviour and chaotic motions of two-axle freight wagons with friction damping. Multibody System Dynamics **8**, 243–255 (2002)
21 True, H., Jensen, J.C.: Parameter study of hunting and chaos in railway vehicle dynamics. Vehicle System Dynamics **23**, 508–521 (1994)
22 Kim, P., Seok, J.: Bifurcation analysis on the hunting behavior of a dual-boige railway vehicle using the method of multiple scales. Journal of Sound and Vibration **329**, 4017–4039 (2010)
23 Polach, O., Kaiser, I.: Comparison of methods analyzing bifurcation and hunting of complex rail vehicle models. Journal of Computational and Nonlinear Dynamics **7**, 041005 (2012)
24 Di Gialleonardo, E., Braghin, F., Bruni, S.: The influence of track modelling options on the simulation of rail vehicle dynamics. Journal of Sound and Vibration **331**, 4246–4258 (2012)
25 Zeng, J.: Simulation of hunting bifurcation and limit cycle of railway vehicle system. Jouranl of the China Railway Society **18**, 13–19 (1996) (in Chinese)
26 Dong, H., Zeng, J., Xie, J.H., et al.: Bifurcation/instability forms of high speed railway vehicles. Science China Technological Sciences **56**, 1685–1696 (2013)
27 Zboinski, K., Dusza, M.: Development of the method and analysis for non-linear lateral stability of railway vehicles in a curved track. Vehicle System Dynamics **44**, 147–157 (2006)
28 Zboinski, K., Dusza, M.: Bifurcation approach to the influence of rolling radius modelling and rail inclination on the stability of railway vehicles in a curved track. Vehicle System Dynamics **46**, 1023–1037 (2008)
29 Zboinski, K., Dusza, M.: Self-exciting vibrations and Hopf's bifurcation in non-linear stability analysis of rail vehicles in a curved track. European Journal of Mechanics-A/Solids **29**, 190–203 (2010)
30 Zboinski, K., Dusza, M.: Extended study of railway vehicle lateral stability in a curved track. Vehicle Systme Dynamics **49**, 789–810 (2011)
31 Zeng, J., Wu, P.B.: Stability Analysis of High Speed Railway Vehicles. JSME International Journal , Series C **47**, (2004)
32 Baker, C.J.: The simulation of unsteady aerodynamic cross wind forces on trains. Journal of Wind Engineering and Industrial Aerodynamics **98**, 88–99 (2010)
33 Baker, C., Hemida H., Iwnicki S., et al.: Integration of cross-wind forces into train dynamic modelling. Proceedings of the Institution of Mechanical Engineers, Part F: Journal of Rail and Rapid Transit **225**, 154–164 (2011)
34 Cheng, Y.C., Chen, C.H., Yang, C.J.: Dynamics analysis of high-speed railway vehicles excited by wind loads. International Journal of Structural Stability and Dynamics **11**, 1103–1118 (2011)
35 Yu, M.G., Zhang, J.Y., Zhang, W.H.: Running attitudes of car body and wheelset for high-speed train under cross wind. Jiaotong Yunshu Gongcheng Xuebao **11**, 48–55 (2011) (in Chinese)
36 Liu, J.L., Yu, M.G., Zhang, J.Y., et al.: Study on running safety of high-speed train under crosswind by large eddy simulation. Journal of the China Railway Society **33**, 13–21 (2011) (in Chinese)
37 Mao, J., Xi, Y.H., Yang, G.W.: Research on influence of characteristics of cross wind field on aerodynamic performance of a high-speed train. Journal of the China Railway Society **33**, 22–30 (2011) (in Chinese)
38 Cheli, F., Desideri, R., Diana, G., et al.: Cross wind effects on tilting trains. 7th World Congress on Railway Research (2006)
39 Baker, C., Cheli, F., Orellano, A., et al.: Cross-wind effects on road and rail vehicles. Vehicle system dynamics **47**, 983–1022 (2009)
40 Yu, M.G., Zhang, J.Y., Zhang, K.Y., et al.: Study on the operational safety of high-speed trains exposed to stochastic winds. Acta Mechanica Sinica **30**, 351–360 (2014)
41 Zeng, X.H., Lai, J.: Hunting stability of high-speed railway vehicle considering the actions of steady aerodynamic loads. Engineering Mechanics **30**, 52–58 (2013) (in Chinese)
42 Shen, Z.Y., Hendick, J.K., Elkins, J.A.: A comparison of alternative creep force models for rail vehicle dynamic analysis. Vehicle System Dynamic **12**, 79–83 (1983)